Stress Distribution Analysis using ANSYS of the Nose Landing Gear of STOL Aircrafts Considering Runway Gradient: A Simulation Study

Bharosh Kumar Yadav[1]*, Ramhit Yadav[2], and K. Sudhakar[3]

[1]Department of Mechanical Engineering, Institute of Engineering, Purwanchal Campus, Tribhuvan University

[2]Department of Physics, Suryanarayan Satyanarayan Morbaita Yadav Multiple Campus, Siraha, Tribhuvan University

[3]Faculty of Mechanical and Automotive Engineering Technology, Universiti Malaysia Pahang

*Corresponding Author: bharosh@ioepc.edu.np

https://doi.org/10.3126/oas.v2i1.65618

Abstract

Landing gear failures are a major cause of aircraft failures because they are an integral part of the aircraft's development. According to the Federal Aviation Administration (FAA), 50% of all aircraft failures occur during take-offs and landing. The landing gear of a short take-offs and landing (STOL) aircraft has had its static and dynamic forces analyzed analytically and numerically. SOLIWORKS is used to model the landing gear, and ANSYS is used to perform the numerical simulation results. Following it, the model is examined for stress and deformation with the boundary conditions and computed loads into account. This study uses structural finite element analysis (FEA) to analyze the nose gear's stress behavior and displacement during landing, as well as to assess the effect of the runway gradient. Utilizing a comprehensive numerical simulation, the landing gear of a real material Twin-Otter STOL aircraft has been demonstrated to be subjected to a dynamic force of 3653.26N, a pneumatic pressure of 1.59MPa, a bead pressure of 7.97MPa, and a vertical force of 1672.31lbs on level runways, or runways with no gradient. These findings will increase the level of confidence of aircraft manufacturers to make necessary appropriate design of STOL aircraft's landing gear. It may can decrease the aircraft accidents and increase human life safety ultimately saving valuable time and resources too.

Keywords: STOL, Twin-Otter, landing gear, runway gradient, numerical simulations

Introduction

Background

One of the trickiest forms of transportation in the modern world is aviation. Short take-off and landing (STOL) aircraft are incredibly adaptable and well-known for their capacity to function in difficult and demanding conditions. An excellent option for uses of these aircrafts, including flight excursions, commercial transportation, and operations in distant locations with difficult weather and topography (Zhang et al., 2023).

The best option for operations in far-flung locations with little runway space, like the Arctic or hilly terrain. The robustness and simplicity of maintenance of small passenger aircraft contribute significantly to their appeal to operators and passengers. These aircraft are a popular option for a variety of aviation tasks, including search and rescue, firefighting, medical evacuation, and short-haul and regional air transportation. Their straightforward, dependable,

and safety-focused design makes them a popular choice. The weather and topography of Nepal make it more practical to operate this aircraft here. Approximately, 25 tiny passenger aircraft, also referred to as Twin-Otters, have been operated in Nepal; currently, there are 6 small passenger aircraft operating in the country (Civil Aviation Authority of Nepal [CAAN], 2019-2020; Ke et al., 2024; Yadav et al., 2020).

Nomenclature of Landing Gear

An aircraft's landing gear is located beneath the fuselage and acts as the vehicle's support system both during take-offs and while it is stationary. The aircraft's front landing gear, sometimes referred to as the nose gear, is made up of various crucial parts that enable it to carry out its intended purpose. The following Figure 1, shows how the Twin Otter's landing gear is assembled:

Figure 1 *Twin Otter Landing Gear Part*
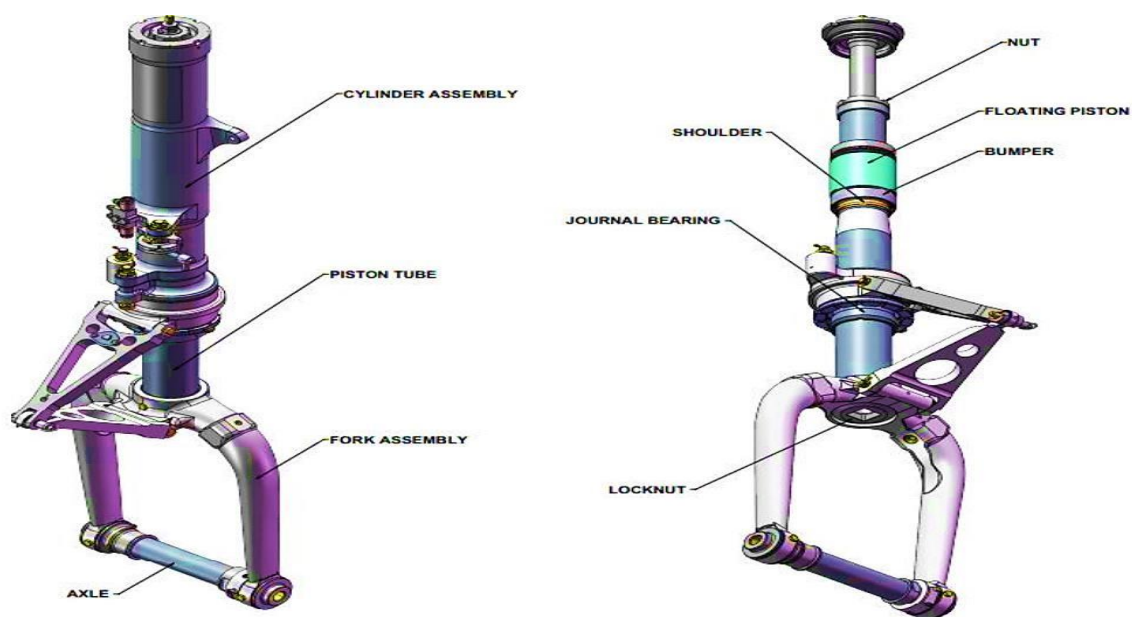
Note. Adopted from Schmidt (2021).

However, most of the parts are not engaged in stress distribution, thus the nose gear of a small passenger aircraft is simplified to serve as a model for the stress analysis, which only considers the parts and designs that are involved in stress distribution. An aircraft's fixed landing gear is made up of the following primary parts such as Tires, Wheels, Brakes, Axles (Gerhardinger et al., 2022; Sonowal et al., 2021).

Shock Absorbers/ Oleo Strut

The small passenger aircraft uses oleo-pneumatic shock absorbers. A shock absorber is composed of up of two chambers, an upper chamber filled with oil and a lower chamber filled with nitrogen or compressed air. Pneumatic forces cushion during ground operation, the piston compresses upon landing, and hydraulic forces release energy during landing. The shock absorber, which is schematically illustrated in Figure 2, is powered by a combination of pneumatic, hydraulic, and frictional forces. As the cylinder's volume decreases and internal pressure increases, there are forces operating on the seal and its contact surface that are frictional, hydraulic, and pneumatic (Hameed et al., 2020).

Figure 2 *Schematic Diagram of Oleo Strut of Landing Gear*
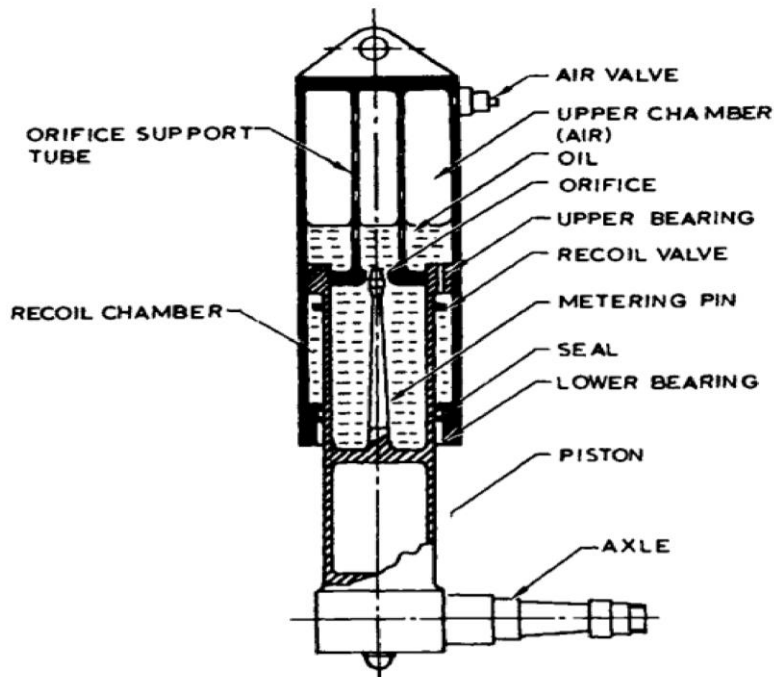
Note. Adopted from Schmidt (2021).

Steering mechanism

When the aircraft is on the ground, it enables the pilot to control its direction. The steering mechanism is not included in the design since it can be disregarded when doing a structural study of the aircraft landing gear. Together, these elements enable the aircraft to land and take off safely and steadily.

Problem statement

One of the main parts of the aeroplane body is the landing gear. It cushions the impact during landing, maintains the structural integrity of the aircraft, and facilitates manoeuvring of the aircraft during ground handling. The landing and take-offs phases of aircraft operation are among the most important ones. Landing gears are now required in designs to enable the greatest amount of impact absorption. Thus, choosing the right material and doing a stress analysis become crucial design factors. According to numerous studies, the majority of collisions occur right after take-off or right after touchdown. The failure of the landing gear is the cause of almost half of aircraft crashes (Bhattarai et al., 2022; Bk, 2017). In Nepal, the majority of twin otters have experienced crashes or mishaps. In Nepal's hilly regions, the majority of runways built have steep slope gradients. The stress distribution becomes increasingly erratic as a result. The landing gear system may sustain damage from the vibration or stress to the point of failure. Some of Nepal's airports along with information on the gradient of the runway, the number of accidents that have occurred there, and the overall number of passenger deaths in Table 1.

Table 1 *Hilly Region Airports of Nepal*

Name of Airport	Elevation (meter)	Location	Runway gradient	Total Accidents	Total Fatality
Tenzing Hillary/ Lukla Airport	2846	Solukhumbu	11.7%= 6.67°	9	23
Jomsom Airport	2736	Mustang	1.75%=1°	3	15
Simikot Airport	2971	Humla	-	4	0

Note. Adapted from Regmi, 2015-11-08.

The majority of STOLs are intended for runways with gradients of no more than 12%. It has also been discovered that the high gradient influences the landing gear's stress. In this particular context, the study concentrated especially on variables related to the development of landing gear stress and the correlation between vertical forces, stress, and gradient.

Research/Knowledge Gap

After conducting a comprehensive literature review, several research gaps were identified. Firstly, there is lack of studies on small passenger aircraft nose landing gear considering runway gradient using computational analysis utilizing ANSYS to evaluate stress distribution. Considering the Nepalese airports and their unique challenges such as Nepal's topography, short-runways, STOL aircraft usage, and operational considerations (Bk, 2017; Gerhardinger et al., 2022; Voskaki et al., 2023).

Research objective

The primary objective of this work is to comprehensively demonstrate the stress behavior of the landing gear under various runway gradient conditions. Specially, the study aims to:

- Evaluate Stress distribution on the landing gear during landing.
- Establish the relation between runway gradient and the reaction forces developed in the Nose Landing Gear.
- Effect of the Runway Gradient on Stress developed in the Landing gear.

Literature Review

The majority of the landing gear's engineering features and design specifications. The development of landing gear design from fundamental concepts to modern designs for both military and commercial aircraft thanks to the comprehensive ideas on current design trends and approaches, together with historical background. Developing the landing gear, the data and formulas can be utilised as a dimension connected to aircraft spare parts and components that are not made public for security and safety reasons (Currey, 1988). The conceptual engineering approach by Mohammad H. Sadraey and Daniel P. Raymer provided comprehensive design considerations for aircraft, including design concepts and major component mathematical equations. Similar to this, the concepts of aircraft design use a system engineering methodology to develop the parameters, including wheelbase, track, and landing gear height ("Aircraft Conceptual Design," 2012; "Aircraft Design Fundamentals," 2012; "Aircraft Weight Distribution," 2012; Kassapoglou, 2013; "Landing Gear Design," 2012; "Preliminary Design," 2012; Raymer, 1992). The comprehensive and the specific study of static and dynamic forces during an aircraft's landing utilizing the Eye-Bar Theory concept to calculate the nose gear's displacement, stress concentration, and distribution during the landing using the FEA Method

(Schmidt, 2021). The material used in aircraft landing gear components by various manufacturers is mentioned and the airworthiness regulations checklist, which lists the prerequisites and limitations for the FEA approach for passenger aircraft landing gear for structural and fatigue safety by S.G. Aftab and his co-authors (Aftab et al., 2022). The effect of increasing aircraft landing weight on tyre performance, landing weight causes stress propagation and tyre deformation, which may result in tyre tearing and blowouts, which airlines should avoid by aircraft damage and crashes (Essienubong, 2018). James N. Daniels performed numerical simulation and experimental study to validate the landing gear equation of motion during action (Daniels, 1996).

The existing literature review reveals a gap in research pertaining to the precise variation of reaction forces in relation to changes in gradient. While several publications and theses have explored various aspects of landing gear design, analysis, and performance, none of them have specifically addressed the investigation of how reaction forces vary when the gradient of the landing surface is altered.

Methodology

The methodology adopted for this research endeavour which is shown in Figure 3. The required data and equations are taken from reliable sources. The whole project is divided into different phases:

Figure 3 *Flowchart describing the methodology of the study*
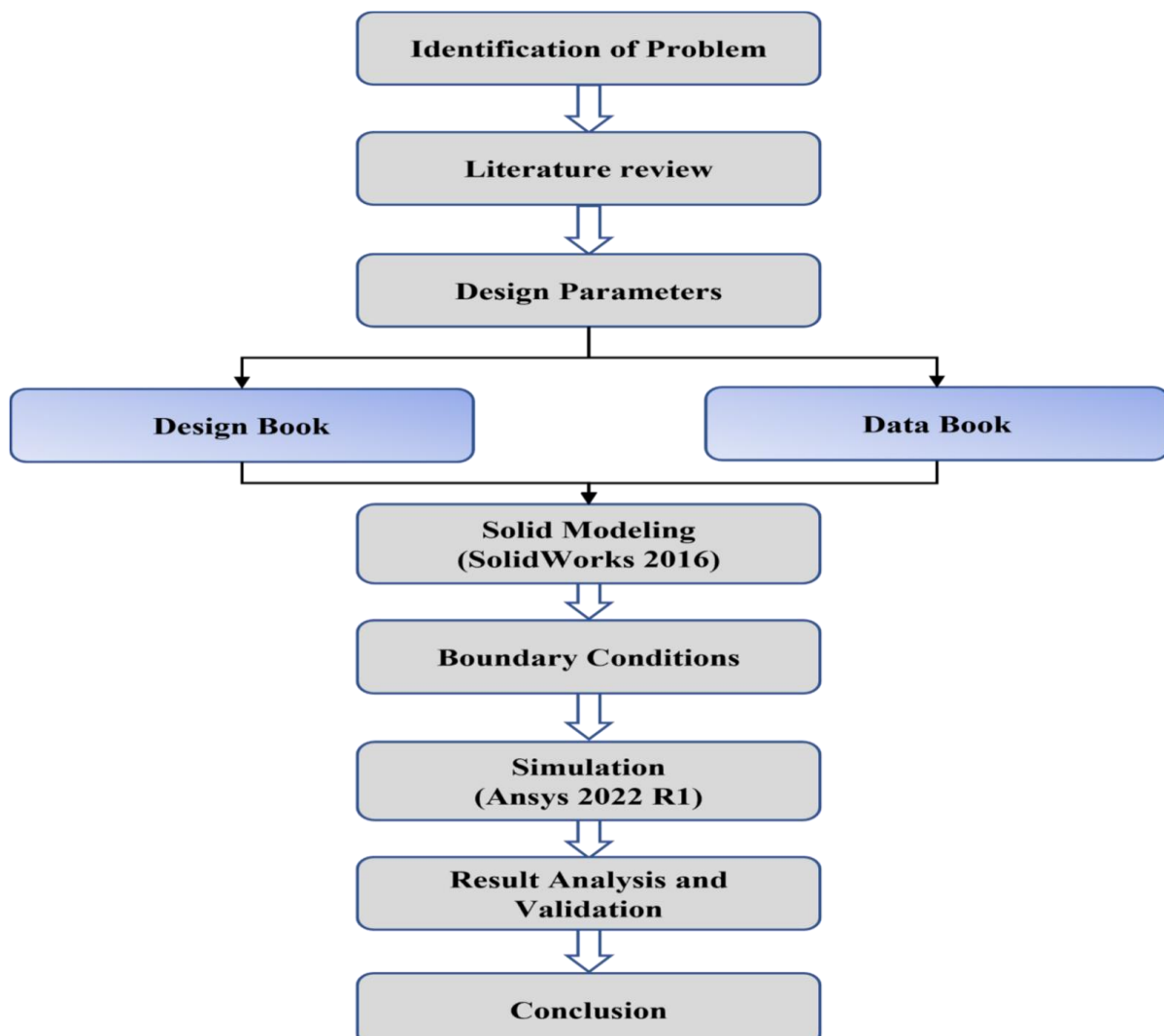
Design Consideration

In terms of safety, the aircraft sector is among the most sensitive & Twin Otter's accessible data is used as a guide (Bach & McNally, 1988; Currey, 1988). The Twin Otter (DHC-6) landing gear part number and the Global Aviation Tyre and Rubber Company data book were used to determine the tire's dimensions, which are displayed in Table 2.

Table 2 *Tires Input Specification*

Parameters	Units
Part Number	217K22-1
Rated Inflation	166 Psi
Static Loaded Radius (SLR) = Rolling Radius (R_r)	9 inches
Flat Tire Radius (FTR)	7.30 inches
Aspect Ratio	0.779
Inflated Dimension	
Maximum Outside Diameter $(D_0)_{max}$	21.25 inches
Minimum Outside Diameter $(D_0)_{min}$	20.6 inches
Maximum Cross-section Width $(W_t)_{max}$	7.2 inches
Minimum Cross-section Width $(W_t)_{min}$	6.8 inches
Maximum Shoulder Diameter $(D_s)_{max}$	19.25 inches
Maximum Shoulder Width $(W_s)_{max}$	6.35 inches
Wheel	
Wheel (Rim) size	22*6.6 inches
Width Between Flanges	5.50 inches
Specified Rim Diameter	10 inches
Flange Height	1 inch
Min Ledge Width	1.80 inches

Note. Sources of table are Book (2022) and Tires (2022).

Stroke Length of Shock Absorber

During the landing of an aircraft, the vertical velocity of the aircraft creates a certain amount of vertical kinetic energy which needs to be absorbed and dissipated safely. To accomplish this, the aircraft is equipped with shock absorbers and tires (Currey, 1988; "Landing Gear Design," 2012; Raymer, 1992; Schmidt, 2021).

The formula for the vertical kinetic energy of the aircraft is:

$$(K.E.)_{Vertical} = \frac{1}{2} \frac{(W_{landing}) \times (v_{vertical})^2}{g} \tag{1}$$

The formula for the energy absorbed is:

$$(K.E.)_{absorbed} = \eta LS = (\eta FS)_{shock\ absorber} + (\eta_t FS_t)_{tire} \tag{2}$$

The formula for tire stroke is given below.

$$S_t = \frac{D_t}{2} - R_r \tag{3}$$

Where,

D_t = Tire Diameter

R_r = Rolling Diameter

Now, we know that during landing the vertical K.E. is equal to absorbed K.E. i.e. $(K.E.)_{Vertical} = (KE)_{absorbed}$

$$\frac{1}{2} \frac{(W_{landing}) \times (v_{vertical})^2}{g} = (\eta FS)_{shock\ absorber} + (\eta_t FS_t)_{tire} \tag{4}$$

Solving we get,

$$S = \frac{(v_{vertical})^2 \times (W_{landing})}{2g\eta F} - \left(\frac{\eta_t}{\eta} \times S_t\right)$$

Landing Gear Load Factor

$$n = \frac{F}{W_{landing}}$$

Thus,

$$S = \frac{(v_{vertical})^2}{2g\eta n} - \left(\frac{\eta_t}{\eta} \times S_t\right) \tag{5}$$

Where n represents load factor also called the limiting load factor or landing gear load factor. $W_{landing}$ includes the payload, fuel weight, Crew weight and weight of the aircraft.

Oleo Strut

Length of Oleo Strut during static condition:

$$L_{oleo} = \frac{S}{0.60} \tag{6}$$

(i.e. for general aviation aircraft)

Length of Oleo Strut during full extension:

$$L_{oleo} = 2.5 \times S \tag{7}$$

Now,

Perpendicular force on oleo strut during landing;

$$(F_{oleo}) = V_f = (n - L)W_{landing}\left(\frac{b'}{d'}\right) \tag{8}$$

Where,

Value of $W_{landing}$ can be obtained from Figure 4;

Figure 4 *CG Range with Fixed Landing Gear*
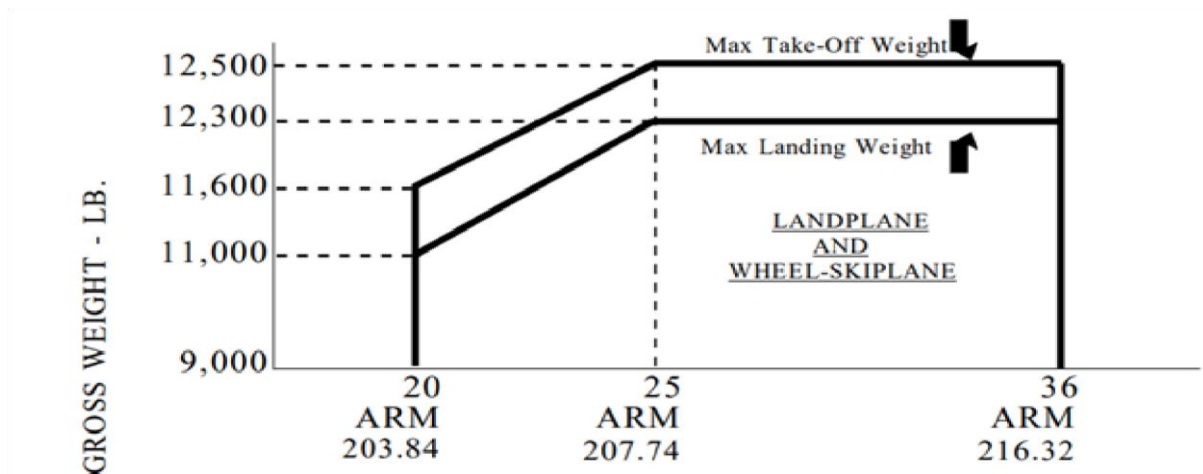
Note. Sources (Currey, 1988; Daniels, 1996; Raymer, 1992).

Oleo Diameter

Internal Oleo Diameter:

$$(D_{oleo})_{int} = 1.3 \sqrt{\frac{4F_{oleo}}{P_{oleo} \times \pi}} \cong 0.035\sqrt{F_{oleo}} \qquad (9)$$

External Oleo Diameter:

$$(D_{oleo})_{ext} = 1.3 \times (D_{oleo})_{int} \qquad (10)$$

Modelling of Landing Gear

The landing gear design and modelling were completed using a SOLIDWORKS 3D model that was based on the parametric input design data from Table 3, as shown in Figure 5.

Figure 5 *Modelling of Twin-Otter (DHC-6) Landing Gear*
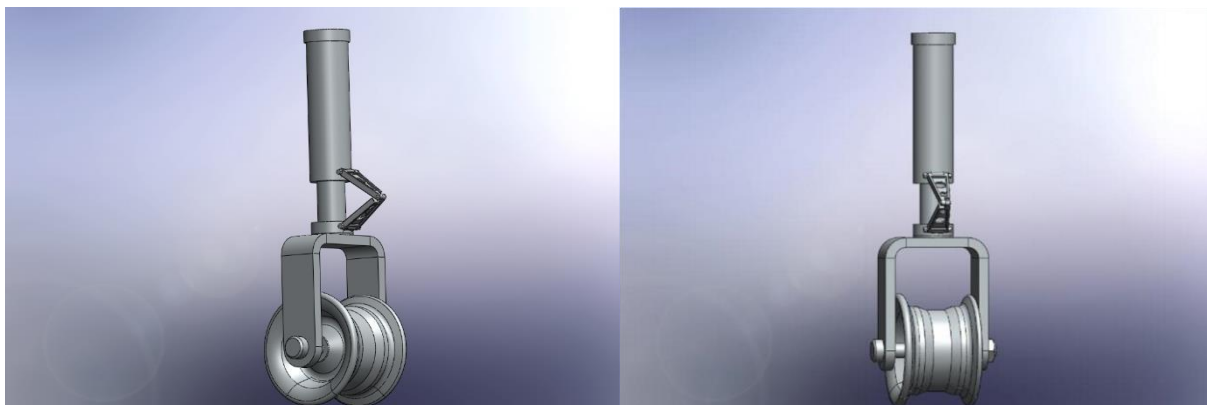
Meshing

To ensure accuracy, FEA solutions were given the right kind and quantity of mesh for each individual part (Yadav et al., 2022). Table 3 summarizes the various element types utilized in meshing structure.

Table 3 *Element Type and Amount*

Parts	Type of element	Elements	Nodes
Outer Cylinder	Tetrahedral	42786	25217
Piston	Tetrahedral	25902	17108
Fork	Tetrahedral	54276	34903
Wheel Hub	Tetrahedral	125578	83428
Axle	Tetrahedral	13408	8048

Note. Source: "Appendix C - Finite element analysis with ANSYS" (2022)

Mesh control is utilized in this numerical simulation study in several distinct locations in order to increase the rate of convergence and yield results that are more precise. For the reason that an element size of 8 mm is chosen and Figure 6 demonstrates the meshed structure.

Figure 6 *Meshed Structure of Landing Structure*
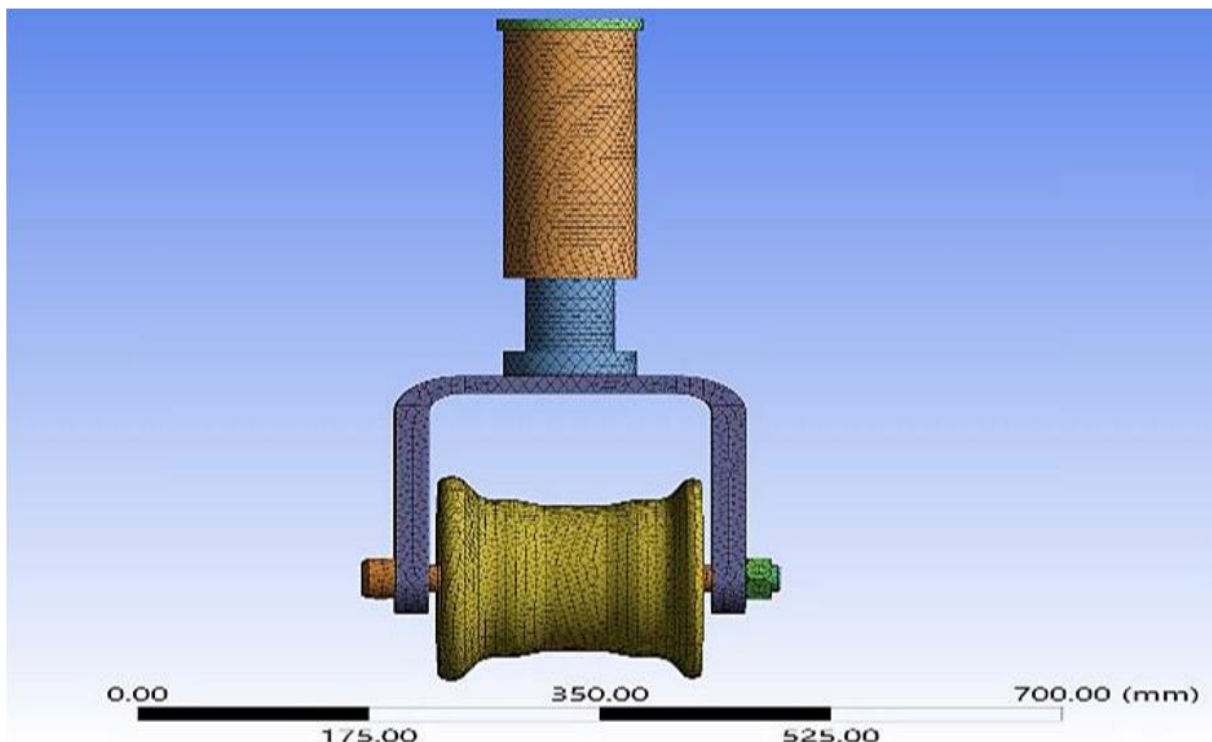
Numerical Simulation

The finite element software ANSYS was utilized for numerical simulations were carried using real material similar with manufacturer of Twin-Otter (DHC-6) Landing Gear under real loading condition felt during landing such as corresponding bead pressure, pneumatic pressure, and loading stress distribution conditions of the aircraft which has been presented in above Table 3. Aluminium provides high corrosion resistance while maintaining structural integrity to support the aircraft (Yadav et al., 2022). The materials selected are shown in Table 4 and comply with the standard specifications supplied by the manufacturers.

Table 4 *Twin-Otter (DHC-6) Landing Gear Material*

Components	Material	Youngs Modulus of Elasticity (GPa)	Density (gm/cm^3)	Ultimate Tensile Strength (MPa)	Yield Strength (MPa)	Poisons ratio
Wheel-Hub	A356	72.4	2.67	234	165	0.33
Axle	AISI-4340	200	7.85	1448	972	0.29
Outer/inner cylinder	300M	205	7.84	1930	1585	0.28
Orifice-plate	300M	205	7.84	1930	1585	0.28
Tapered-Metering pin	300M	205	7.84	1930	1585	0.28
Torque-arm	TIMETAL-834	120	4.55	1050	930	0.32
Fork	7075-T6-Aluminum	72	2.8	572	503	0.33

Note. Source: Armaan et al. (2020)

Loading Conditions (Static)

Taking into account the three main loading conditions: Ground Vertical Force on the landing gear nose-gear, Corresponding Bead-Pressure, and Pneumatic-Pressure when analyzing the stress distribution.

Vertical Force on the Nose Gear. The ground reaction force is established when the airplane first touches the runway. The Figure7 presents the landing configuration, depicting the imminent contact between the nose gear and the ground. The measurements a, b, and d were obtained from the Twin-Otter data book, enabling the determination of a', b', and d'-while inclined (Currey, 1988; Federal Aviation Authority's [FAA], 2011; Gao et al., 2024; Hagins et al., 2007; Liang et al., 2022).

Figure 7 Levelled Landing with Inclined Reactions
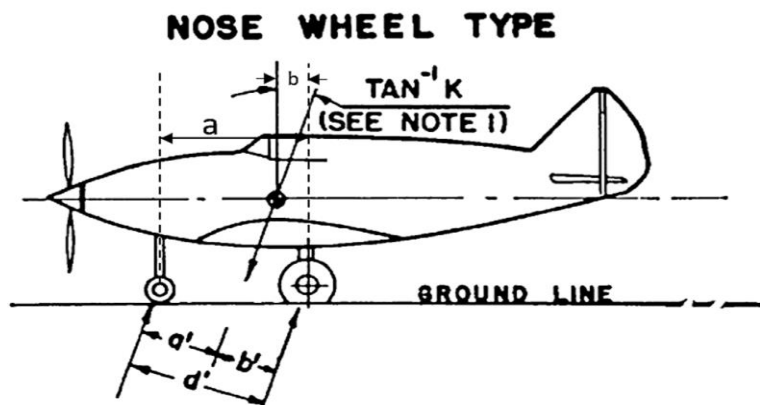
Reaction-angle (θ) is given by Schmidt (2021) and Sonowal et al. (2021):

$$(\theta) = \tan^{-1}(K) \tag{11}$$

Where, K = 0.33; for $W_{landing} > 6{,}000\ lbs$

Subsequently, we get (FAA, 2011) from Figure 7;

$\theta = 18.26°$

Now, the general vertical force can be calculated for levelled runway i.e., zero gradient as:

$$V_f = (n - L)W_{landing}\left(\frac{b'}{d'}\right) = 7672.31\ lbs \tag{12}$$

Corresponding Bead Pressure. Now, the above vertical forces will be converted to pressure using the Eye-bar theory, which will be applied at the bead seat location of the tire on the wheel hub. This pressure will be distributed on the bottom portion of the wheel, across angle α according to the contact patch region theory (Schmidt, 2021; Sonowal et al., 2021; Sun et al., 2024).

The required formula for the conversion is:

$$W_\circ = \frac{V_f.\pi}{b_w.R_b.4.\alpha} \tag{13}$$

$$\text{where,}\quad \alpha = 2\cos^{-1}\left(1 - \frac{h}{\left(\frac{D_{\circ\ max}}{2}\right)}\right),\quad h = \text{Tire stroke } (S_t) \tag{14}$$

$$= 64.21^0$$

Thus, Bead Pressure as:

$$(W_\circ) = 1155.74\ \text{psi} = 7.97\ \text{Mpa} \tag{15}$$

Pneumatic Pressure. The initial air pressure, the area exposed to the air pressure, and the compression ratio, as described by the polytropic law for gas compression given below (Gao et al., 2024; Schmidt, 2021; Sonowal et al., 2021):

$$\frac{P_2}{P_1} = \left[\frac{V_1}{V_2}\right]^n$$

Where, n=polytropic index for air inside cylinder=1.1

$$P_2 = P_1 \times \left[\frac{V_1}{V_2}\right]^n \tag{16}$$

We have, $\tag{17}$

$$A_a = \pi \times \frac{((D_{oleo})_{int})^2}{4}$$

$$= 7.383\ inch^2$$

Initial Pneumatic Volume; $\tag{18}$

$$(V_1) = ((L_{oleo})_{fe} - S) \times A_a$$

$$= 86.012\ inch^3$$

Fully compressed Pneumatic Volume

$$(V_2) = V_1 - A_a\big((L_{oleo})_{fe} - (L_{oleo})_s\big) \tag{19}$$

$$= 38.244 \ inch^3$$

The initial pressure in the oleo strut is 95psi at full extension. Finally, we get; $P_2 = 231.7 \ psi = 1.59 \ MPa$

Thus, the pneumatic pressure at fully-compressed conditions is 1.59 MPa.

Loading Conditions (Dynamic)

The landing gears encounter additional dynamic loads during take-off and landing. The nose gear feels the impact forces when the aeroplane makes contact with the runway during landing, it carries the largest dynamic load. However, it absorbs the forces produced during the retardation phase, the main landing gear bears the largest dynamic load during take-off. Both static and dynamic loads must be taken into account in order to correctly assess the overall loads on the landing gears (Chaudhary, 2021; Jiang et al., 2023; Paletta et al., 2015).

$$(F_n)_{dyn} = \frac{Wlanding \times (\propto_L) \ \frac{H_{cg}}{\cos(\theta_S)}}{d' \times g} \tag{20}$$

Where;

$$\alpha_L = \text{deacceleration due to braking} = \frac{\text{Change in velocity}}{\text{time taken}} = \frac{u_L - v_L}{t_l}$$

Twin-Otter's aircraft need a minimum runway length of 2500 feet. Dynamic force can be computed as follows using equation 3.18: Dynamic force $(F_{dyn}) = 3653.26 \ N$.

According to the loading circumstances, the point of application of these forces and its direction are illustrated in Figure 8: (a), (b), and (c), respectively. Along the anticipated angle of the tire's contact with the runway surface, the bead seat portion receives the bead seat pressure. Similar to this, the rim and wheel hub encounter force that is equally distributed throughout the area upon landing because to the inflation pressure present in the tyre. Moreover, dynamic load forces at the point of maximal compression during landing touch.

Figure 8 *Beat-Inflation-Pressure and Dynamic Loading*
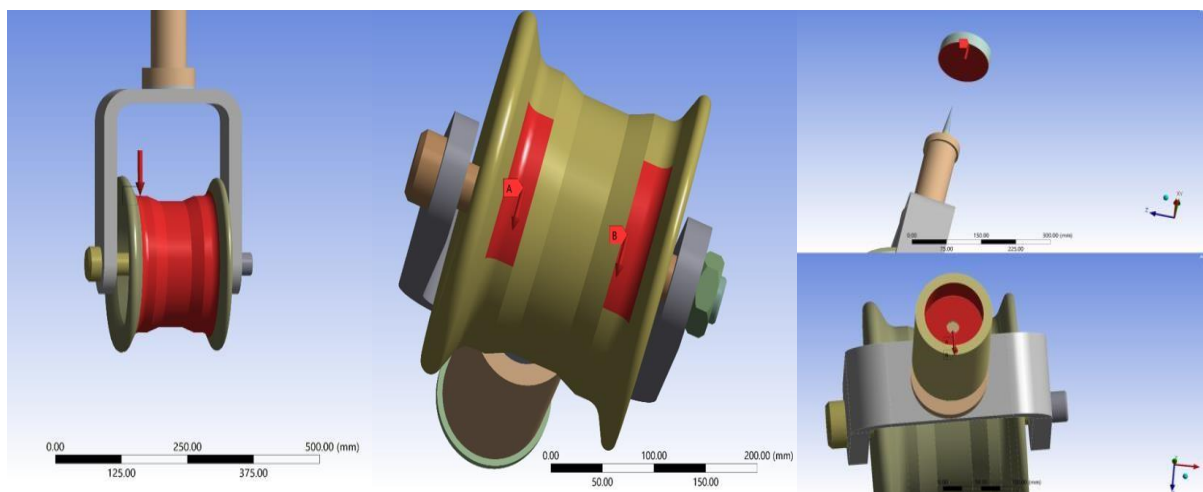
(a). Beat-seat-Pressure   (b). Inflation-pressure   (c). Dynamic-load

Boundary Conditions

We only used bonded conditions in this research work because our primary focus was on structural analysis. In this case, the bolt and hole diameters match, and the inner piston and the outer cylinder's internal diameter have an identical interaction. An overview of all the contact connections utilized during the analysis is given in Table 5, along with information on how each was simulated.

Table 5 *Twin-Otter DHC-6 Landing Gear Components*

Surfaces/bodies	Type of contact	Comments
Fork/Axle	Bonded	Axle is bolted to the ends of a fork to prevent rotational motion.
Wheel & Axle	Bonded	The wheel rotates about the Axle.
Piston/Outer cylinder	Bonded	The piston slides inside the outer cylinder.
Fork/Piston	Bonded	The force during landing is transferred from the fork to piston of the oleo strut for shock absorption.

Note. Source (Eret et al., 2015).

Fixture Component of Landing Gear. Landing gear would behave under particular loads and climatic circumstances the points that need to be fixed (Arunagiri et al., 2022).

In this instance, the outer cylinder's top-cap surface will be fixed as indicated by the figure below, allowing the load to be supplied at the bottom in addition to the pneumatic forces depicted in Figure 9.

Figure 9 *The Upper and the Lower Surface of Gear*
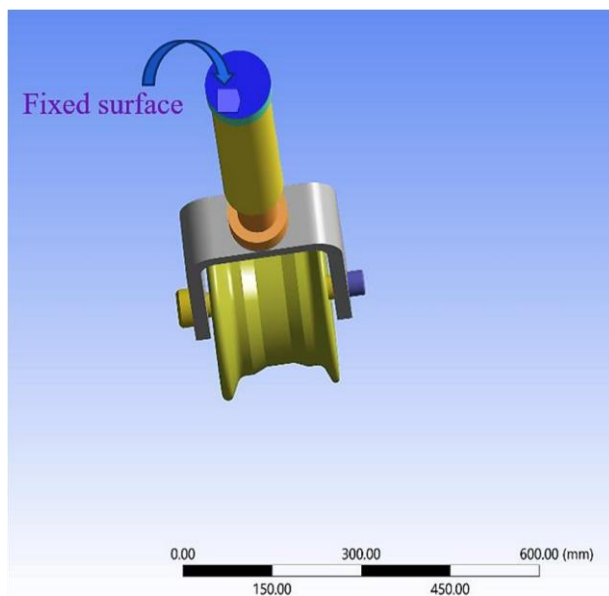
Figure 9:(a). The upper surface   Figure 9:(b). The Lower surface
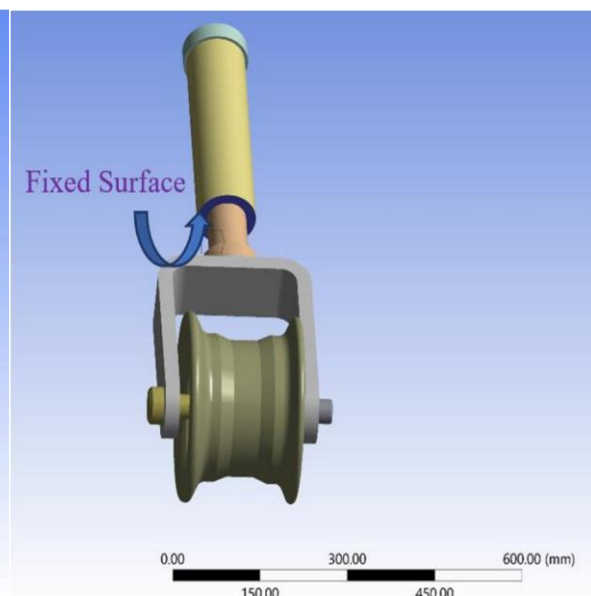
Result and Observations

This section shows the results of the modelling of the DHC-6 aircraft's landing gear using SOLIDWORKS and numerical simulations that show the stress distribution in the landing gear axle, the deformation in the landing gear nose, and the entire landing gear using ANSYS explicit software. Relationship has been approved in accordance with the Federal Aviation Authority's (FAA) standards for landing gear on small aircraft and airport gradient angles or slopes (FAA, 2011).

Stress Distribution

The result indicated that the maximum equivalent stress (Von-Mises stress) during landing occurs in the axle of the nose wheel assembly which is shown in Figure 10. The static structural stress distribution in nose landing gear during landing on the levelled runway is 280.25 MPa.

Figure 10 *Stress Distribution*
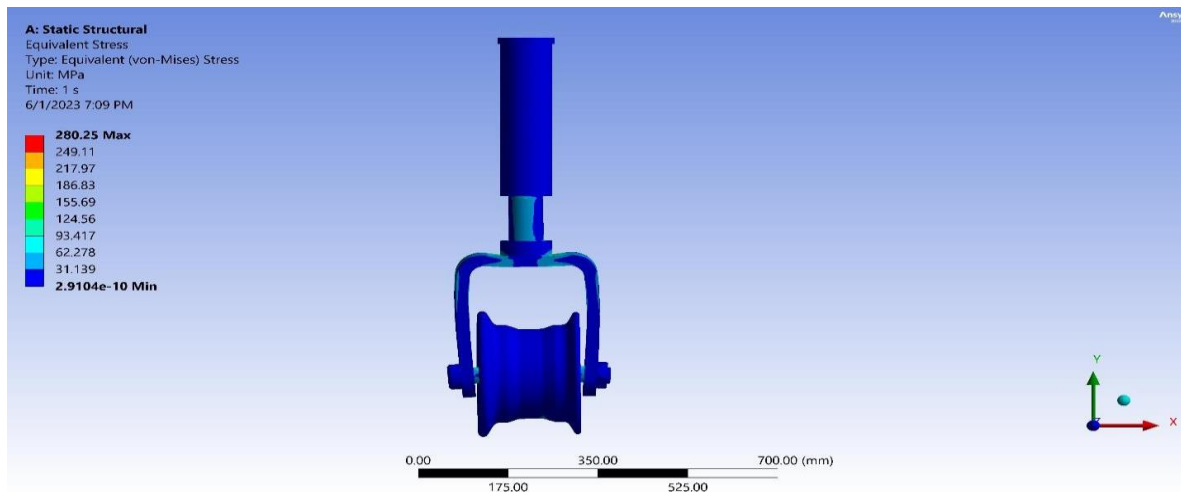
The area of most prominent stress in the axle at the wheel-axle contact surface can be identified by the bright red hue in Figure 11. It has been found that the maximum stress is same as the static structural stress distribution in nose landing gear during landing on the levelled which is considerably within the FAA's limitations.

Figure 11 *Distribution of Stress in the Axle*
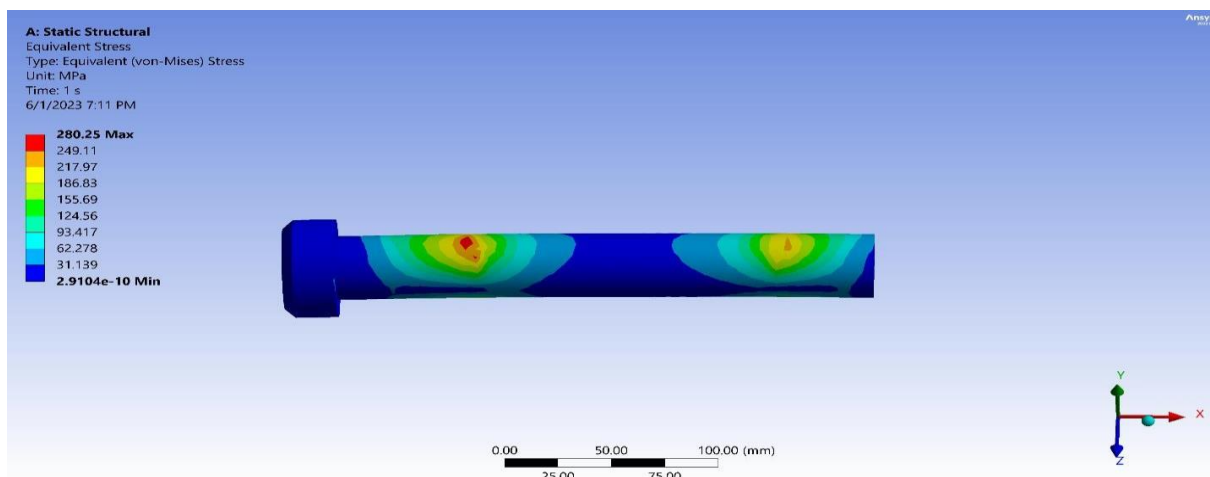
Deformation of the Landing Gear's Nose

The nose landing gear deformation has been shown in the Figure-12. A value of 2.4093 mm has been estimated for the most significant deformation. It therefore makes obvious that the most deformation could be seen at the wheel's bottom location because the outer cylinder's upper surface is fixed during the numerical simulation tests.

Figure 12 *Distortion of the Nose of the Landing Gear*
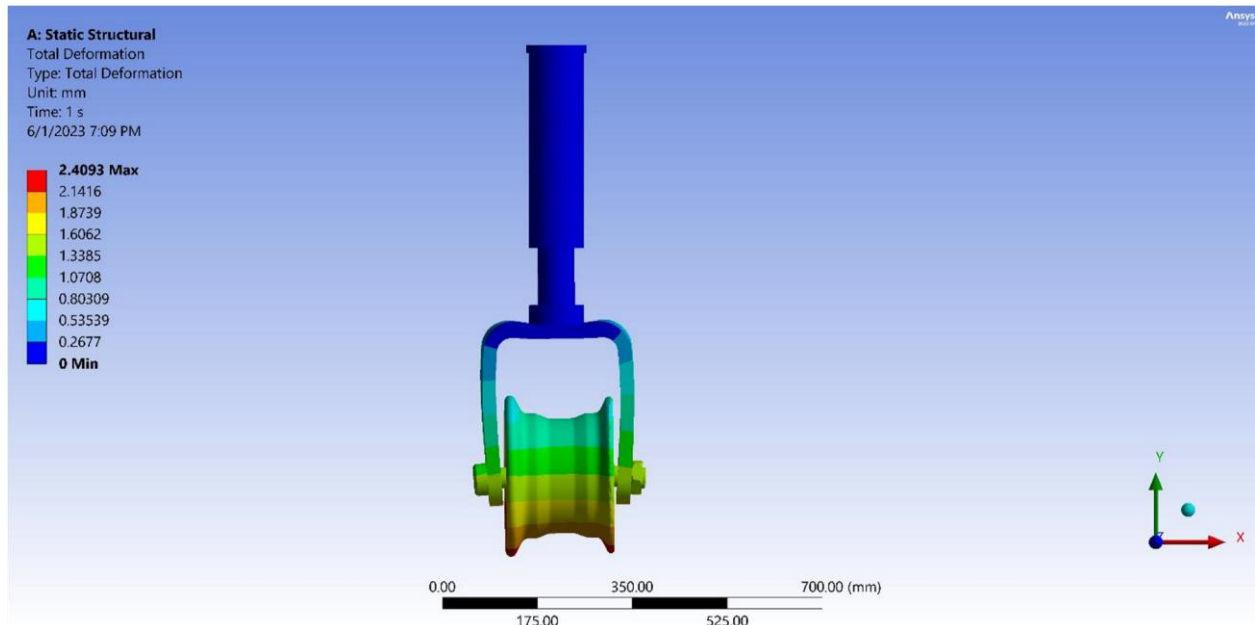
Deformation of the Wheel-hub

The area of highest deformation can be observed by the bright red hue in Figure-13 rim's surface.

Figure 13 *Deformation of the Wheel-hub*
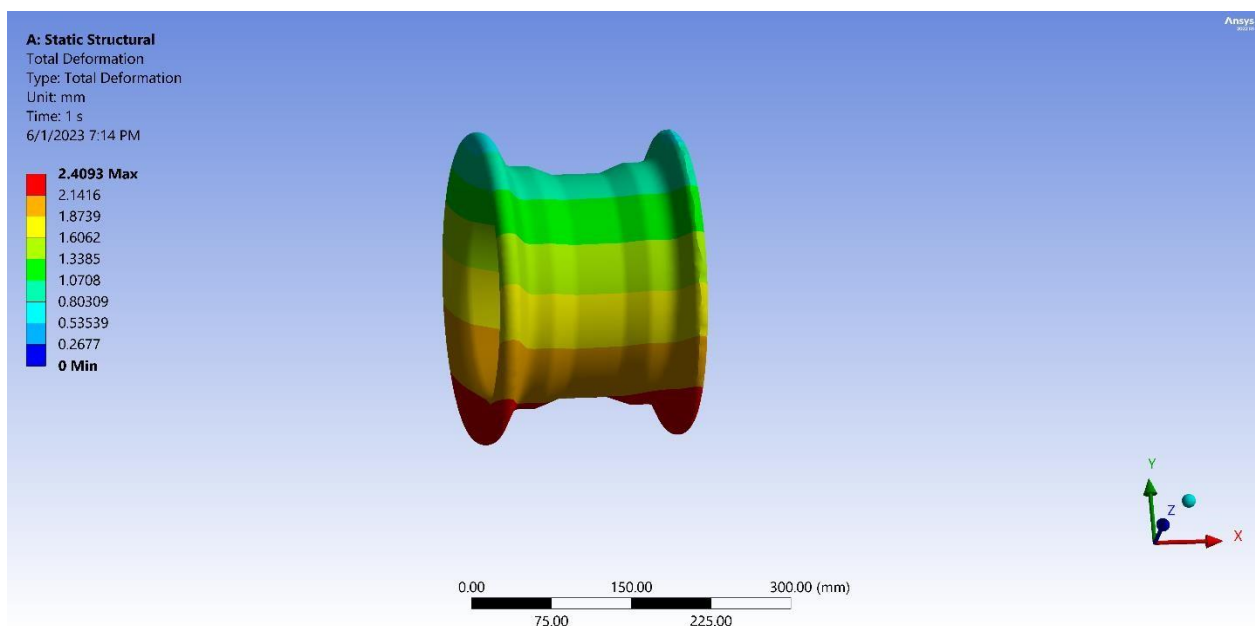
The relationship between V_f and θ_s by utilising Figure 4 and the governing equations 1-20 to determine the vertical force and gradients. The study is constrained to a gradient of 12% since FAA regulations allow for an optimal gradient of 12% (FAA, 2011).

Equations 11-15 establish the connection between gradient and maximum-bead-pressure (W_o). The graph between W and θ_s has been generated is depicted in Figure 14 and 15, respectively.

Figure 15 *Vertical Force Vs Gradient Angle*
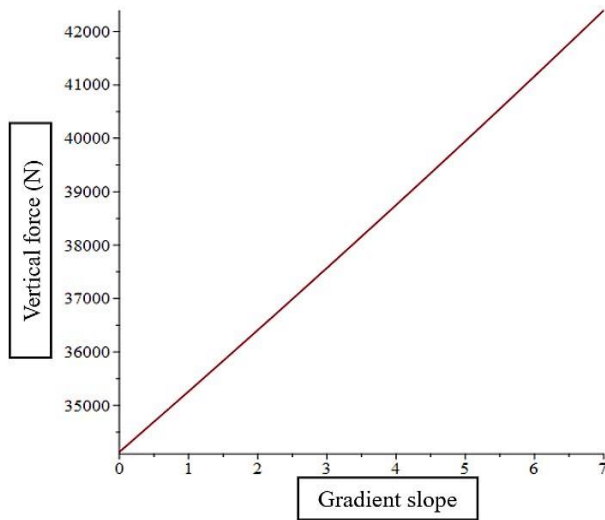
Figure 14 *Maxm^{m} Bead Pressure Vs Gradient Slope*
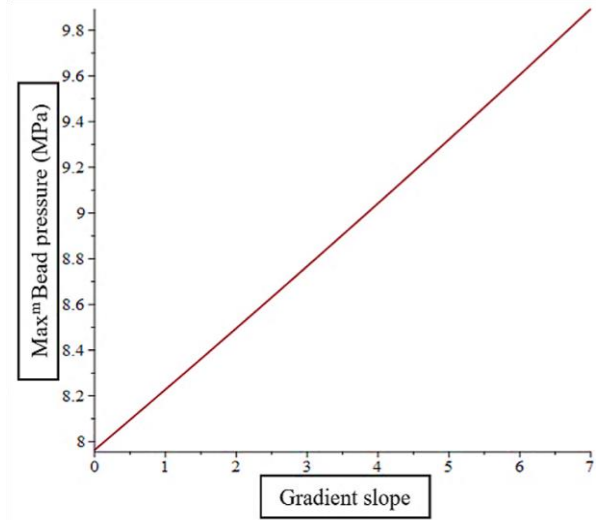
Figure 16 illustrates the relation between gradient angle and dynamic force utilizing equation 11-20.

Figure 16 *Dynamic-force Vs Gradient-slope*
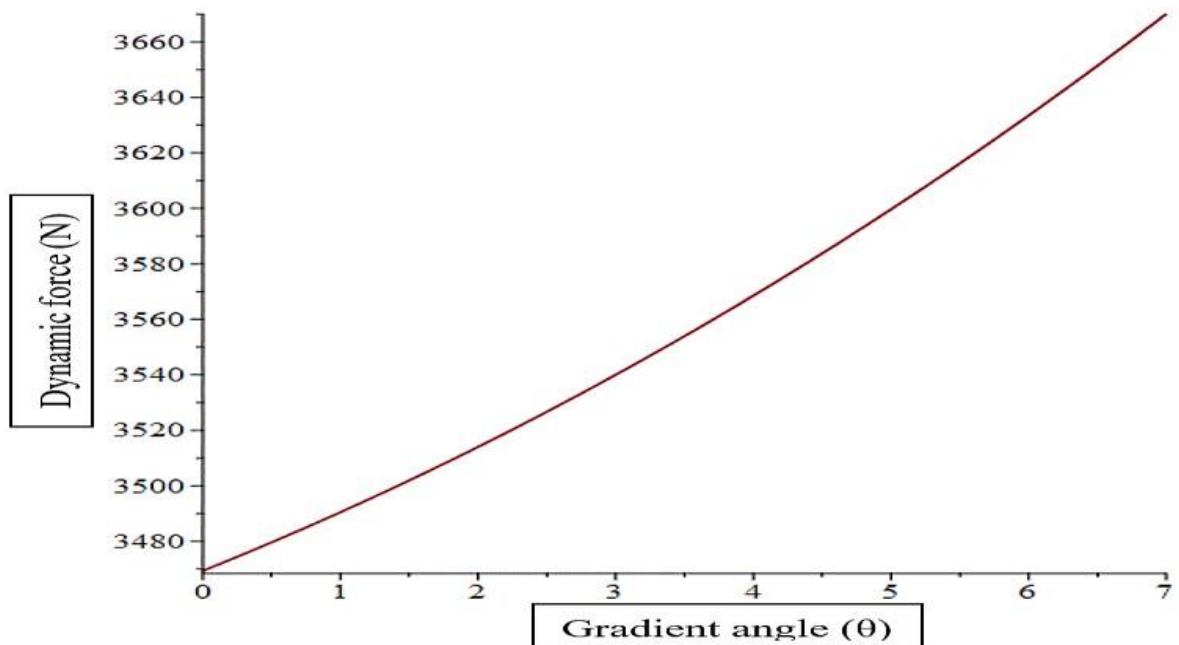
The stress varies as a result of its dependence on all forces, including dynamic and vertical forces with vary slope which is presented in Table 6. The dynamic force variation with gradient for a Twin-Otter (DHC-6) standard runway, as specified by the FAA.

Table 6 *Variation in the Nose Landing Gear's Maximum Stress in Response to a Gradient in the Dynamic Force*

Gradient (%)	Slope (degree)	$F_{dynamic}$ (Newton)	Max Stress (MPa)
0	0	3469.33	280.02
1	0.5729	3481.15	285.34
2	1.1457	3493.75	290.44
3	1.7183	3507.13	296.05
4	2.2906	3521.30	301.5
5	2.8624	3536.28	306.96
6	3.4336	3552.06	312.08
7	4.0041	3568.65	317.54
8	4.5739	3586.07	323
9	5.1427	3604.32	328.47
10	5.7105	3623.42	333.94
11	6.2772	3643.36	339.75
12	6.8427	3664.16	344.89

According to the graph, the maximum equivalent stress and runway gradient have an approximately linear relations; the stress increased by 5.3-5.5MPa for each percentage of gradient which is shown in Figure 17.

Figure 17 *Maximum Equivalent Stress on the Runway and Gradient Percentage*
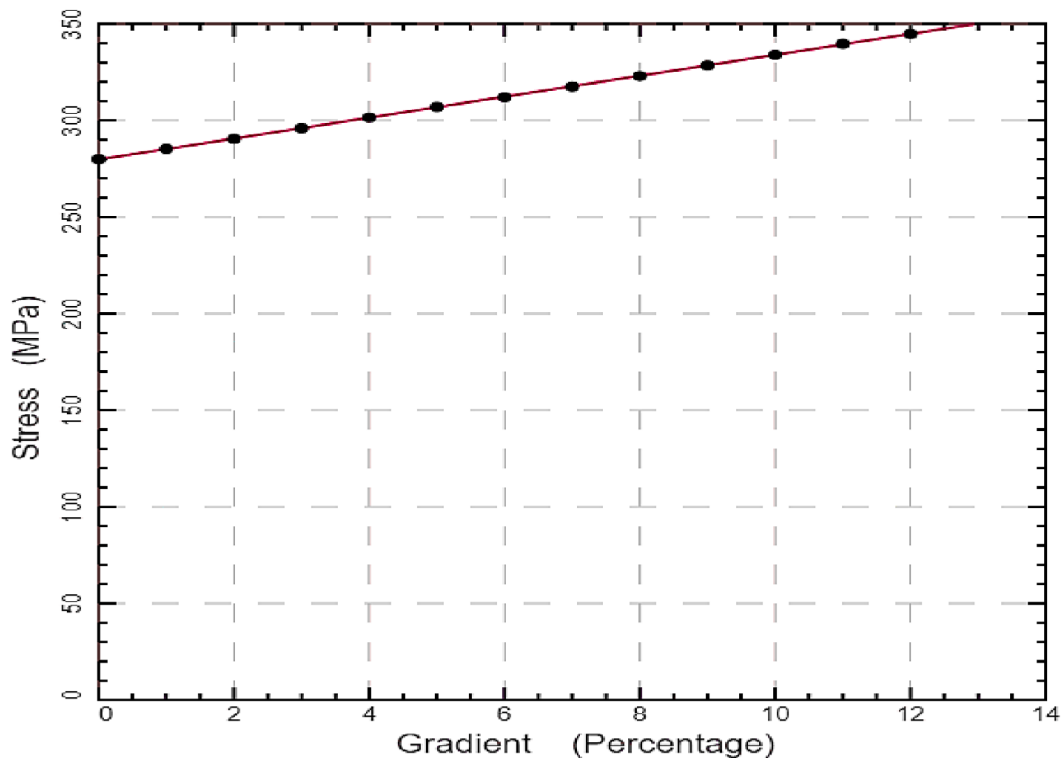
Conclusion and Future Works

In conclusion, this research analysis highlights the significance of understanding the function of nose landing gears and determining the timing of maximum loading scenarios and stress distribution of the landing gear's vertical force on the nose gear, corresponding bead pressure, and pneumatic pressure statically. The following are the significant findings from the study:

1.   The stress distribution analysis of the nose landing gear of STOL-DHC-6 Twin-Otter aircraft considering runway gradient which are commonly used in Nepal has been studied for the first time.

2.   The design and numerical simulation were completed using a SOLIDWORKS and ANSYS respectively using real material of the landing gear.

3.   The comprehensive numerical simulation studies found dynamic force ($F_{Dynamic}$) 3653.26 N, Pneumatic pressure 1.59 MPa, Bead pressure 7.97 MPa, and Vertical force on the nose gear of the landing gear as 1672.31 lbs on levelled runways i.e. zero gradient.

4.   Most importantly, this research work also reveals the increasing nature of maximum equivalent stress with an increase in gradient, emphasizing the need to consider this factor in design evaluations. These findings will increase the level of confidence of aircraft manufacturers to make necessary appropriate design of STOL aircraft. It may can decrease the aircraft accidents and increase human life safety ultimately saving valuable time and resources too. This would enable a broader understanding of the performance characteristics and potential failures across different landing gear designs.

Further study is needed to perform experimental tests to validate with numerical simulation test results to ensure the real-world applicability, conducting physical testing on the landing gear system under various gradient conditions is recommended. Experimental validation would help verify the accuracy of the analytical with the practical insights.

Acknowledgements

References

Aftab, S. G., Sirajuddin, Sreedhara, B., Ganesh, E., Babu, N. R., & Aithal, S. K. (2022). Finite element analysis of a passenger aircraft landing gear for structural and fatigue safety. *Materials Today: Proceedings, 54*, 152-158. https://doi.org/10.1016/j.matpr.2021.08.199

Appendix C - Finite element analysis with ANSYS. (2022). In S. Muftu (Ed.), *Finite element method* (pp. 475-482): Academic Press.

Armaan, A., Keshav, S., & Srinivas, G. (2020). A step towards safety: Material failure analysis of landing gear. *Materials Today: Proceedings, 27*, 402-409. https://doi.org/10.1016/j.matpr.2019.11.245

Arunagiri, P., Vijayakumar, Ayesha Khan, M., & Jani, S. P. (2022). Structural analysis and materials deformations of landing gear. *Materials Today: Proceedings, 60*, 2240-2244. https://doi.org/10.1016/j.matpr.2022.03.310

Bhattarai, A., Dhakal, S., Gautam, Y., Bhattarai, N., Jha, B., & Sharma, U. (2022). Perception of safety culture in the Nepalese aviation industry: A factor analysis approach.

Transportation Research Interdisciplinary Perspectives, 16, 100723. https://doi.org/10.1016/j.trip.2022.100723

Bk, Y. (2017). Aircraft collisions and bird strikes in Nepal between 1946-2016: A case study. *Journal of Aeronautics & Aerospace Engineering, 06*(04). https://doi.org/10.4172/21689792.1000203

Book, G. A. D. (2022)). Three-part tire specification. *The Goodyear Tire & Rubber Company 200 Innovation Way Akron Ohio 44316.*

Civil Aviation Authority of Nepal. (2019-2020). Annual report.

Chaudhary, R. (2021). Investigation on structural dynamics of landing gear. *Materials Today: Proceedings, 46*, 9-15. https://doi.org/10.1016/j.matpr.2020.03.324

Currey, N. S. (1988). Aircraft landing gear design principles and practices. *American Institute of Aeronautics & Ast (1988).*

Daniels, J. N. (1996). *A method for landing gear modeling and simulation with experimental validation.*

Eret, P., Kennedy, J., & Bennett, G. J. (2015). Effect of noise reducing components on nose landing gear stability for a mid-size aircraft coupled with vortex shedding and free play. *Journal of Sound and Vibration, 354*, 91-103. https://doi.org/10.1016/j.jsv.2015.06.022

Essienubong, I. A. (2018). Finite element analysis of aircraft tire behaviour under overloaded aircraft landing phase. *Aeronautics and Aerospace Open Access Journal, 2*(1). https://10.15406/aaoaj.2018.02.00026

Federal Aviation Authority's. (2011). Code of Federal Aviation. *14 CFR Ch. I (1–1–11 Edition).*

Gao, X., Zheng, Y., Du, X., Shan, Z., Jia, B., & Lu, X. (2024). Effect of clearance position of torque link structure on nose landing gear shimmy. *International Journal of Non-Linear Mechanics, 159*, 104616. https://doi.org/10.1016/j.ijnonlinmec.2023.104616

Gerhardinger, D., Abramović, B., Fratrović, T., & Domitrović, A. (2022). Landing gear leg fatigue life analysis for light aircraft. *Transportation Research Procedia, 64*, 14-24. https://doi.org/10.1016/j.trpro.2022.09.003

Hagins, M., Pappas, E., Kremenic, I., Orishimo, K. F., & Rundle, A. (2007). The effect of an inclined landing surface on biomechanical variables during a jumping task. *Clinical Biomechanics, 22*(9), 1030-1036. https://doi.org/10.1016/j.clinbiomech.2007.07.012

Hameed, A., Zubair, O., Shams, T. A., Mehmood, Z., Javed, A., & Mehmood, Z. (2020). Failure analysis of a broken support strut of an aircraft landing gear. *Engineering Failure Analysis, 117*, 104847. https://doi.org/10.1016/j.engfailanal.2020.104847

Jiang, Y., Feng, G., Tang, H., Zhang, J., & Jiang, B. (2023). Effect of Coulomb friction on shimmy of nose landing gear under time-varying load. *Tribology International, 188*, 108828. https://doi.org/10.1016/j.triboint.2023.108828

Kassapoglou, C. (2013). AIRCRAFT DESIGN aerospace series list design and analysis of composite structures: With applications to aerospace structures. *Willey A John Wiley and Sons, Ltd, Publication.*

Ke, Y., Wu, X., Nie, L., Yao, Z., & Chen, Y. (2024). Synchronizing train, aircraft, shuttle, and passenger flows in intermodal timetabling: A time–space network-based formulation and a decomposition algorithm using Alternating Direction method of multipliers. *Transportation Research Part C: Emerging Technologies, 159*, 104464. https://doi.org/10.1016/j.trc.2023.104464

Landing Gear Design. (2012). In *Aircraft Design* (pp. 479-545).

Liang, Z., Lv, C., Zhu, S., & Ge, D. (2022). Guidance for precision landing on asteroid using active hopping trajectory. *Acta Astronautica, 198*, 320-328. https://doi.org/10.1016/j.actaastro.2022.06.003

Paletta, N., Dmytriv, A., Belardo, M., Cristillo, D., & Pecora, M. (2015). Landing gear concept and dynamic landing loads of the unmanned space re-entry vehicle USV3. *Procedia Engineering, 114*, 38-45. https://doi.org/10.1016/j.proeng.2015.08.030

Preliminary Design. (2012). In *Aircraft Design* (pp. 93-159).

Raymer, D. P. (1992). Aircraft design: A conceptual approach. *AIAA Education Series*. https://doi.org/0930403-51-7

Regmi, R. P. (2015-11-08). Aviation hazards over the Jomsom airport of Nepal as revealed by numerical simulation of local flows. *Journal of Institute of Science and Technology*, *19*(1), 111–120. https://doi.org/10.3126/jist.v19i1.13836

Schmidt, R. K. (2021). *The design of aircraft landing gear*: SAE International.

Sonowal, P., Pandey, K. M., & Sharma, K. K. (2021). Design and static analysis of landing gear shock absorber of commercial aircraft. *Materials Today: Proceedings, 45*, 6712-6717. https://doi.org/10.1016/j.matpr.2020.11.1032

Sun, X., Xue, J., Zhou, J., Wang, Z., Wang, W., & Zhang, M. (2024). Design and validation of a variable camber wing structure. *Chinese Journal of Aeronautics, 37*(2), 1-11. https://doi.org/10.1016/j.cja.2023.09.004

Tires, G. A. (2022). Good year aviation data book. *The Goodyear Tire & Rubber Company 200 Innovation Way Akron Ohio 44316*.

Voskaki, A., Budd, T., & Mason, K. (2023). The impact of climate hazards to airport systems: A synthesis of the implications and risk mitigation trends. *Transport Reviews, 43*(4), 652-675. https://doi.org/10.1080/01441647.2022.2163319

Yadav, B. K., Jahangiri, M., & Singh, D. (2022). Experimental and numerical simulation to validate critical perforation velocity on a flat plate aluminium alloy 6061. *Advances in Materials Science and Engineering, 2022*, 3707200. https://doi.org/10.1155/2022/3707200

Yadav, B. K., Rauniyar, P. K., Sudhakar, K., Bajracharya, T. R., & Priya, S. S. (2020). Sustainable green campus in NEPAL: 3E analysis. *International Journal of Low Carbon Technologies, 16*(2), 531-542. https://doi.org/10.1093/ijlct/ctaa088

Zhang, Y., Xu, J., Pan, R., Li, Y., Ma, Z., & Huang, S. (2023). Numerical investigation of short takeoff and landing exhaust system using bypass dual throat nozzle. *Aerospace Science and Technology, 138*, 108316. https://doi.org/10.1016/j.ast.2023.108316